

# High and anomalous thermal conductivity in monolayer $\text{MSi}_2\text{Z}_4$ semiconductors

Yan Yin,<sup>†</sup> Min Yi,<sup>\*,†,‡</sup> and Wanlin Guo<sup>\*,†</sup>

<sup>†</sup>*Institute for Frontier Science, Institute of Nanoscience, State Key Lab of Mechanics and Control of Mechanical Structures & Key Lab for Intelligent Nano Materials and Devices of Ministry of Education & College of Aerospace Engineering, Nanjing University of Aeronautics and Astronautics (NUAA), Nanjing 210016, China*

<sup>‡</sup>*National Laboratory of Solid State Microstructures, Nanjing University, Nanjing 210093, China*

E-mail: yimin@nuaa.edu.cn; wlguo@nuaa.edu.cn

## Abstract

The lattice thermal conductivity ( $\kappa$ ) of newly synthesized two-dimensional (2D)  $\text{MoSi}_2\text{N}_4$  family and its associated abnormality are anatomized by *ab initio* phonon Boltzmann transport calculations.  $\kappa$  of  $\text{MoSi}_2\text{N}_4$  and  $\text{WSi}_2\text{N}_4$  is found over  $400 \text{ Wm}^{-1}\text{K}^{-1}$  at 300 K.  $\kappa$  of  $\text{MoSi}_2\text{Z}_4$  ( $\text{Z} = \text{N, P, As}$ ) obeys Slack's rule of thumb, decreasing by one order of magnitude from  $\text{Z} = \text{N}$  to  $\text{Z} = \text{As}$  with  $46 \text{ Wm}^{-1}\text{K}^{-1}$ . However, in  $\text{MSi}_2\text{N}_4$  ( $\text{M} = \text{Mo, Cr, W, Ti, Zr, Hf}$ ), the variation of  $\kappa$  with respect to  $\text{M}$  is anomalous, i.e. deviating from Slack's classic rule. For  $\text{M}$  in the same group,  $\kappa$  of  $\text{MSi}_2\text{N}_4$  is insensitive to the average atomic mass, Debye temperature, phonon group velocity, and bond strength owing to the similar phonon structure and scattering rates.  $\text{MSi}_2\text{N}_4$  with heavy group-VIB  $\text{M}$  even possesses a three to four times higher  $\kappa$  than that with light group-IVB  $\text{M}$ , due to its much stronger  $\text{M-N}$  and exterior  $\text{Si-N}$  bonds and thus one order of magnitude lower phonon scattering rates. Nevertheless, this abnormality could be traced

to an interplay of certain basic vibrational properties including the bunching strength and flatness of acoustic branches and their nearby optical branches, which lie outside of the conventional guidelines by Slack. This work predicts high  $\kappa$  of 2D  $\text{MSi}_2\text{Z}_4$  for thermal management and provides microscopic insight into deciphering the anomalous  $\kappa$  of layered 2D structures.

**Keywords:** 2D  $\text{MoSi}_2\text{N}_4$  family, Lattice thermal conductivity, Phonon vibration and scattering, *ab initio* calculations, Phonon Boltzmann transport equation

The work was submitted to ACS Applied Materials & Interfaces and was accepted for publication in Sep 6, 2021.

## 1. INTRODUCTION

Two-dimensional (2D) semiconductors, such as black phosphorene (BP)<sup>1</sup>, semiconducting transition metal dichalcogenides (TMDs)<sup>2</sup> and group-IVA and -VIA compounds,<sup>3,4</sup> have aroused considerable interests in various nanoelectronic devices, due to their outstanding electrical properties, flexibility, and controllable bandgap. The interesting thermal transport properties in 2D semiconductors induced by quantum confinement effect provides new directions for thermal energy control and management, such as interface thermal resistance,<sup>5,6</sup> thermoelectric<sup>7,8</sup> and thermal transistor devices.<sup>9,10</sup> On the other hand, thermal dissipation is increasingly significant in integrated circuits since the power dissipation density and high-temperature hot spots cause the performance degradation as well as long-term reliability issues. 2D semiconductors with high thermal conductivity ( $\kappa$ ) are critical for keeping nanoelectronic devices cool by removing the high-density dissipation. Up to now, compared with the high  $\kappa$  of zero-bandgap graphene ( $3000\text{--}5000\text{ Wm}^{-1}\text{K}^{-1}$ )<sup>11</sup> and insulated hexagonal boron nitride ( $600\text{ Wm}^{-1}\text{K}^{-1}$ ),<sup>12</sup> high  $\kappa$  of 2D semiconductors is mainly in carbon- or boron-based materials.<sup>13–16</sup> Nevertheless, the exploration of new 2D semiconductors and their thermal properties never stops.

Very recently, layered 2D  $\text{MoSi}_2\text{N}_4$  and  $\text{WSi}_2\text{N}_4$  have been synthesized successfully by introducing silicon to passivate the high-energy surfaces of non-layered molybdenum nitride during chemical vapor deposition growth.<sup>17</sup> After the breakthrough discovery, the  $\text{MA}_2\text{Z}_4$  family has been theoretically predicted.<sup>18</sup> The  $\text{MA}_2\text{Z}_4$  phase contains early transition metal elements (M), silicon or germanium (A), and group-VA elements (Z). In the large  $\text{MA}_2\text{Z}_4$  family there exist affluent and interesting physical and chemical properties, for instances, piezoelectricity, photocatalysis, and strain-induced change of electrical properties.<sup>19–25</sup> The monolayer  $\text{MoSi}_2\text{N}_4$  shows high optical transmittance (97.6%), which is comparable to that of graphene (97.7%). Meanwhile, the excellent mechanical properties (Young’s modulus of  $491.4 \pm 139.1$  GPa and breaking strength of  $65.8 \pm 18.3$  GPa) and the stability under ambient conditions laid out the promising usage of  $\text{MoSi}_2\text{N}_4$  in the future.<sup>17</sup> The high  $\kappa$  of  $\text{MoSi}_2\text{N}_4$  and  $\text{WSi}_2\text{N}_4$  are appealing for the thermal management in semiconductor devices.<sup>19,26</sup> Mortazavi and coworkers<sup>19</sup> proposed that thermal conductivity of  $\text{MA}_2\text{Z}_4$  is attributed to the core atomic mass, phonon group velocity and phonon-phonon scattering. Apart from these, many vital factors, such as average atomic mass, Debye temperature, phonon transport properties, and even the structure itself, which are critical for deciphering the underlying mechanism of  $\kappa$  of  $\text{MSi}_2\text{Z}_4$ , still remain to be explored.

In this paper, the effects of different M or Z atoms on structure and phononic nature of  $\text{MSi}_2\text{Z}_4$  are discussed. Then, the thermal transport properties are revealed by solving phonon Boltzmann transport equation (BTE). The role of several possible factors (e.g. average atomic mass, Debye temperature, phonon group velocity, phonon-phonon scattering properties, bond strength, etc.) in determining  $\kappa$  of  $\text{MSi}_2\text{Z}_4$  is exhaustively examined. We find that  $\text{MoSi}_2\text{N}_4$  and  $\text{WSi}_2\text{N}_4$  possess a high  $\kappa$  greater than  $400 \text{ W}^{-1}\text{K}^{-1}$  at 300 K. In Slack’s rule,<sup>27,28</sup> nonmetallic crystals with high thermal conductivity usually have four characters which are (1) low atomic mass, (2) strong bonding, (3) simple crystal structure, and (4) low anharmonicity. However, the variation of  $\kappa$  with respect to M atoms is anomalous and does not strictly obey Slack’s classic rule. According to the rule of thumb by Slack,

$\kappa$  decreases with increasing average atomic mass ( $\bar{m}$ ) and decreasing Debye temperature ( $\Theta_D$ ). In contrast,  $\kappa$  of  $\text{MSi}_2\text{N}_4$  with larger  $\bar{m}$  and smaller  $\Theta_D$  (M in group-VIB) is even 3–4 times higher than that with smaller  $\bar{m}$  and larger  $\Theta_D$  (M in group-IVB). Moreover,  $\kappa$  of  $\text{MSi}_2\text{N}_4$  remains at the same level irrespective of  $\bar{m}$  and  $\Theta_D$  when M atoms are in the same group. More microscopic details on deciphering the high and anomalous  $\kappa$  of  $\text{MSi}_2\text{Z}_4$  are also comprehensively examined.

## 2. RESULTS AND DISCUSSION

### 2.1. Lattice structure and phonon band structure

Herein, we investigate eight types of 2D  $\text{MSi}_2\text{Z}_4$ , including the experimentally synthesized  $\text{MoSi}_2\text{N}_4$  and  $\text{WSi}_2\text{N}_4$ . The monolayer  $\text{MSi}_2\text{Z}_4$  can be considered as a sandwich structure that one 2H  $\text{MoS}_2$ -type  $\text{MZ}_2$  layer is inserted into an  $\alpha$ -InSe-type  $\text{Si}_2\text{Z}_2$  layer. The perspective and side views of the structure are shown in Fig. 1. There are four nonequivalent atoms in the unit cell, namely, M, Si, Z1 and Z2. The M represents transition metal elements (Mo, W, Cr, Ti, Zr, Hf) and the Z represents group-VA elements (N, P, As). Three different bonds formed by these atoms are denoted by Bond 1 (M-Z1 bond), Bond 2 (Si-Z1 bond) and Bond 3 (Si-Z2 bond). The structure parameters after full relaxation are listed in Table 1. The lattice constant of  $\text{MoSi}_2\text{N}_4$  is  $a = b = 2.91 \text{ \AA}$ , which is in line with the previous experimental results ( $2.909 \text{ \AA}$ ). For conveniently exploring the effect of different atoms on the properties of  $\text{MSi}_2\text{Z}_4$ , we divide the eight structures into two groups, i.e.  $\text{MSi}_2\text{N}_4$  and  $\text{MoSi}_2\text{Z}_4$ .

As shown  $\text{MoSi}_2\text{Z}_4$  in Table 1, the lattice constants of  $\text{MoSi}_2\text{P}_4$  and  $\text{MoSi}_2\text{As}_4$  is 3.47 and 3.62  $\text{\AA}$ , which are about 19.2% and 24.3% larger than that of  $\text{MoSi}_2\text{N}_4$ . Accordingly, the bonds are also elongated with the increasing period number of elements Z from N to P to As. The effective thickness ( $h_{\text{eff}}$ ) along vertical direction is defined as the sum of distance between top and bottom atoms and vdW diameter of outmost Z2 atom.  $h_{\text{eff}}$  of  $\text{MoSi}_2\text{N}_4$ ,



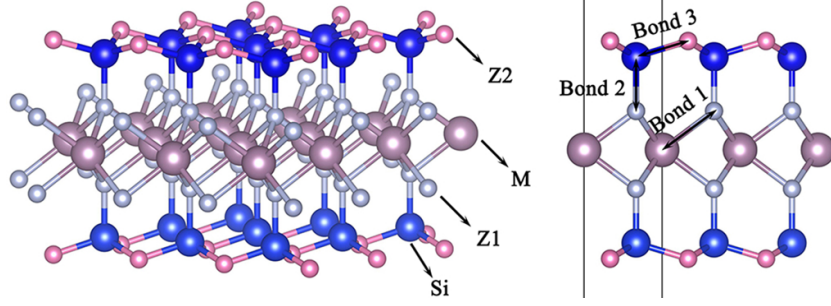


Figure 1: Lattice structure of  $\text{MSi}_2\text{Z}_4$ . M is Mo, Cr, W, Ti, Zr or Hf atom, and Z is N, P, or As atom.

$\text{MoSi}_2\text{P}_4$  and  $\text{MoSi}_2\text{As}_4$  are 10.01, 13.17 and 13.90 Å, respectively. In contrary, for  $\text{MSi}_2\text{N}_4$  all the lattice constant, bond length and effective thickness do not change remarkably with respect to M atoms. With PBE calculation, the eight types of  $\text{MSi}_2\text{Z}_4$  are all semiconductors with a band gap around of 0.49–2.08 eV, as shown in Fig. S1. Apart from  $\text{MoSi}_2\text{P}_4$  and  $\text{MoSi}_2\text{As}_4$  with narrow direct band gap, other configurations are indirect semiconductors. The band gaps calculated by both GGA and HSE functionals are list in Table S1, indicating the semiconductor nature of  $\text{MSi}_2\text{Z}_4$  family.

Table 1: Lattice parameters ( $a = b$ ), effective thickness ( $h_{\text{eff}}$ ), bond lengths, average mass ( $\bar{m}$ ), group velocity ( $\nu$ ) near  $\Gamma$  point, and Debye temperature ( $\Theta_{\text{D}}$ ) of acoustic branches in 2D  $\text{MSi}_2\text{Z}_4$ .

	$a = b$	$h_{\text{eff}}$	Bond 1	Bond 2	Bond 3	$\bar{m}$	$\nu_{\text{ZA}}$	$\nu_{\text{TA}}$	$\nu_{\text{LA}}$	$\Theta_{\text{D}}$
	(Å)	(Å)	(Å)	(Å)	(Å)	(amu)	(km/s)	(km/s)	(km/s)	(K)
$\text{MoSi}_2\text{N}_4$	2.91	10.01	2.10	1.75	1.76	29.73	4.10	6.33	10.30	434.78
$\text{MoSi}_2\text{P}_4$	3.47	13.17	2.46	2.24	2.25	39.43	4.03	4.25	6.04	212.21
$\text{MoSi}_2\text{As}_4$	3.62	13.94	2.56	2.36	2.37	64.5	3.07	3.09	4.44	144.92
$\text{WSi}_2\text{N}_4$	2.91	10.01	2.10	1.75	1.76	42.29	4.62	5.45	8.55	336.28
$\text{CrSi}_2\text{N}_4$	2.84	9.87	2.00	1.75	1.73	23.45	3.88	6.72	11.20	485.71
$\text{TiSi}_2\text{N}_4$	2.93	9.91	2.07	1.75	1.77	22.86	3.92	6.82	10.90	264.24
$\text{ZrSi}_2\text{N}_4$	3.04	10.05	2.18	1.75	1.82	29.06	4.03	5.77	8.93	208.94
$\text{HfSi}_2\text{N}_4$	3.02	10.00	2.16	1.75	1.81	41.52	3.73	4.83	8.32	168.00

The phonon dispersion spectrums of  $\text{MSi}_2\text{Z}_4$  are shown in Fig. 2. There are 3 acoustic branches (including ZA, TA and LA branches) and 18 optical branches due to 7 atoms in the unit cell. No imaginary frequency of each branch indicates the dynamic stability. The phonon frequency range is around 0–30 THz in  $\text{MSi}_2\text{N}_4$  ( $\text{M} = \text{Mo}, \text{W}, \text{Cr}, \text{Ti}, \text{Zr}, \text{Hf}$ ), but it is only 0–17.02 THz in  $\text{MoSi}_2\text{P}_4$  and 0–14 THz in  $\text{MoSi}_2\text{As}_4$ . Comparing the average mass ( $\bar{m}$ ) of each structure in Table 1, one can find large  $\bar{m}$  induces obvious softening of phonon branches. In the phonon density of states (PhDOS) (Fig. S2), heavy atoms occupy the low frequency region while light ones contribute to the high frequency region. Compared with N, P or As is heavier and thus PhDOS and the whole phonon spectrum of  $\text{MoSi}_2\text{P}_4$  or  $\text{MoSi}_2\text{As}_4$  notably shift to the lower frequency. However, the case for  $\text{MSi}_2\text{N}_4$  is entirely different. Firstly, the whole frequency range of phonon spectra of  $\text{MSi}_2\text{N}_4$  remains almost the same in spite of different M atoms or  $\bar{m}$ . Secondly, heavier M or larger  $\bar{m}$  prominently results in flatter lower-frequency acoustic branches, only when M in the same group. Thirdly, M in group-IVB leads to much flatter acoustic branches (especially ZA branch) than M in group-VIB. The flatter and lower-frequency ZA branch indicates that the out-of-plane vibration and interatomic force of  $\text{MSi}_2\text{N}_4$  ( $\text{M} = \text{Ti}, \text{Zr}, \text{Hf}$ ) along the  $z$  direction are weaker.

## 2.2. High $\kappa$ of $\text{MSi}_2\text{N}_4$ with Group-VIB M

The calculated  $\kappa$  of  $\text{MSi}_2\text{Z}_4$  as a function of temperature ( $T$ ) is presented in Fig. 3(a). In the whole temperature range,  $\kappa$  of  $\text{MoSi}_2\text{N}_4$  is the highest and that of  $\text{MoSi}_2\text{As}_4$  is the lowest. At room temperature (300 K),  $\kappa$  of  $\text{MoSi}_2\text{N}_4$  is up to  $417 \text{ Wm}^{-1}\text{K}^{-1}$ , which is higher than that of most other 2D materials, such as h-BAs ( $310 \text{ Wm}^{-1}\text{K}^{-1}$ ),<sup>29</sup> hydrogenated borophene ( $368 \text{ Wm}^{-1}\text{K}^{-1}$ ),<sup>30</sup> monolayer GaGeTe ( $58 \text{ Wm}^{-1}\text{K}^{-1}$ ),<sup>31</sup> 2H transition metal dichalcogenides (e.g.  $\text{WS}_2$  ( $142 \text{ Wm}^{-1}\text{K}^{-1}$ ),  $\text{MoS}_2$  ( $23 \text{ Wm}^{-1}\text{K}^{-1}$ ),  $\text{MoSe}_2$  ( $54 \text{ Wm}^{-1}\text{K}^{-1}$ )),<sup>32–34</sup> and group-IVA and -VIA compounds (e.g.  $\text{GeS}$  ( $9.8 \text{ Wm}^{-1}\text{K}^{-1}$ ),  $\text{PbSe}$  ( $0.26 \text{ Wm}^{-1}\text{K}^{-1}$ )).<sup>4,35</sup> But it is lower than that of graphene ( $3000\text{--}5000 \text{ Wm}^{-1}\text{K}^{-1}$ ),<sup>11,36</sup> Carbon-based nitrides ( $820 \text{ Wm}^{-1}\text{K}^{-1}$ )<sup>37</sup> and hexagonal boron nitrogen (h-BN,  $600 \text{ Wm}^{-1}\text{K}^{-1}$ ).<sup>38</sup>

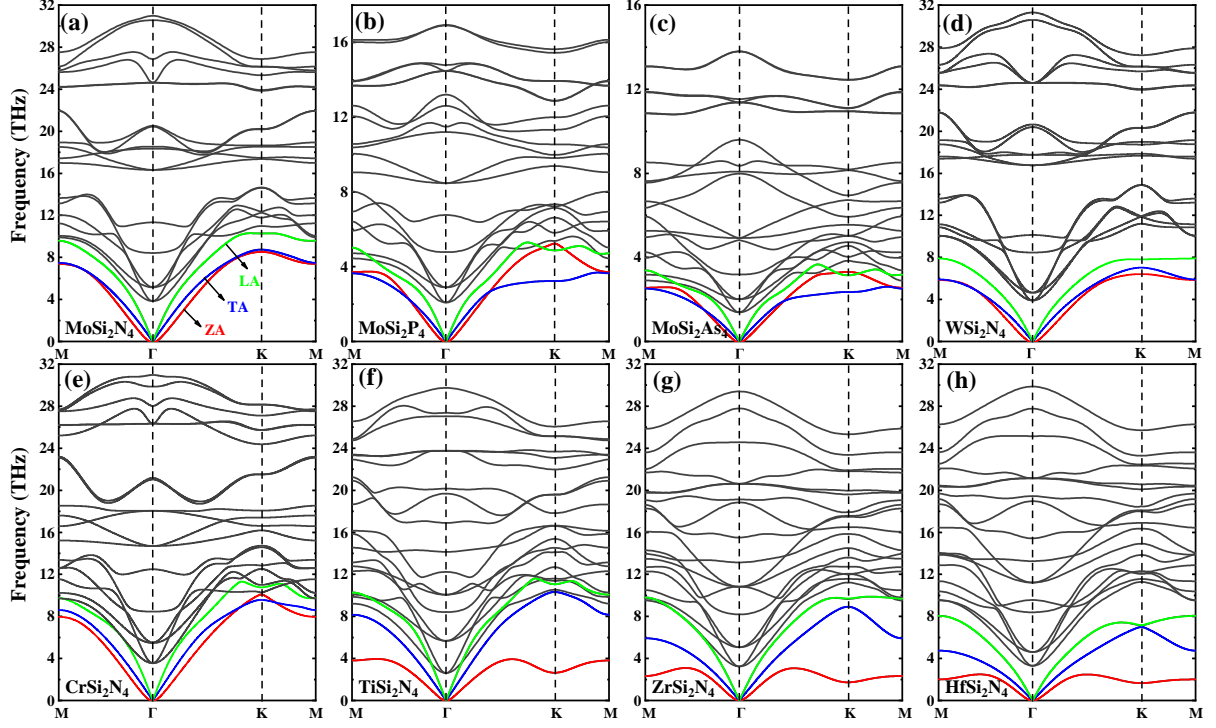


Figure 2: Phonon dispersion spectrum of 2D  $\text{MSi}_2\text{Z}_4$ : (a)  $\text{MoSi}_2\text{N}_4$ , (b)  $\text{MoSi}_2\text{P}_4$ , (c)  $\text{MoSi}_2\text{As}_4$ , (d)  $\text{WSi}_2\text{N}_4$ , (e)  $\text{CrSi}_2\text{N}_4$ , (f)  $\text{TiSi}_2\text{N}_4$ , (g)  $\text{ZrSi}_2\text{N}_4$  and (h)  $\text{HfSi}_2\text{N}_4$ .

Besides, the room temperature  $\kappa$  of  $\text{WSi}_2\text{N}_4$  and  $\text{CrSi}_2\text{N}_4$  are 401 and 348  $\text{Wm}^{-1}\text{K}^{-1}$ , respectively. As shown in Fig. 3 (b), the thermal conductive range of  $\text{MSi}_2\text{Z}_4$  is wider than that of group-IVA and -VIA compounds or TMDs. And such high  $\kappa$  of group-VIB  $\text{MSi}_2\text{N}_4$  is promising for heat conductors and thermal management in semiconductor devices. The underlying microscopic mechanism for the high  $\kappa$  in  $\text{MSi}_2\text{N}_4$  with group-VIB M will be anatomized in Section 2.4.

### 2.3. Large reduction of $\kappa$ in $\text{MoSi}_2\text{Z}_4$

At 300 K,  $\kappa$  of  $\text{MoSi}_2\text{Z}_4$  remarkably decreases from 417  $\text{Wm}^{-1}\text{K}^{-1}$  of  $\text{MoSi}_2\text{N}_4$  to 116  $\text{Wm}^{-1}\text{K}^{-1}$  of  $\text{MoSi}_2\text{P}_4$  to 46  $\text{Wm}^{-1}\text{K}^{-1}$  of  $\text{MoSi}_2\text{As}_4$  (Fig. 3). In fact, h-BZ ( $\text{Z} = \text{N, P, As}$ )<sup>12</sup> and graphene-like BZ ( $\text{Z} = \text{H, F, Cl}$ )<sup>30</sup> also show the similar phenomenon. But their reduction in  $\kappa$  with respect to Z is much smaller than that in  $\text{MoSi}_2\text{Z}_4$ . For instance,  $\kappa$  of h-BAs at 300 K is 40% of that of h-BN, whereas  $\kappa$  of  $\text{MoSi}_2\text{As}_4$  is only 11% of that of  $\text{MoSi}_2\text{N}_4$ . The

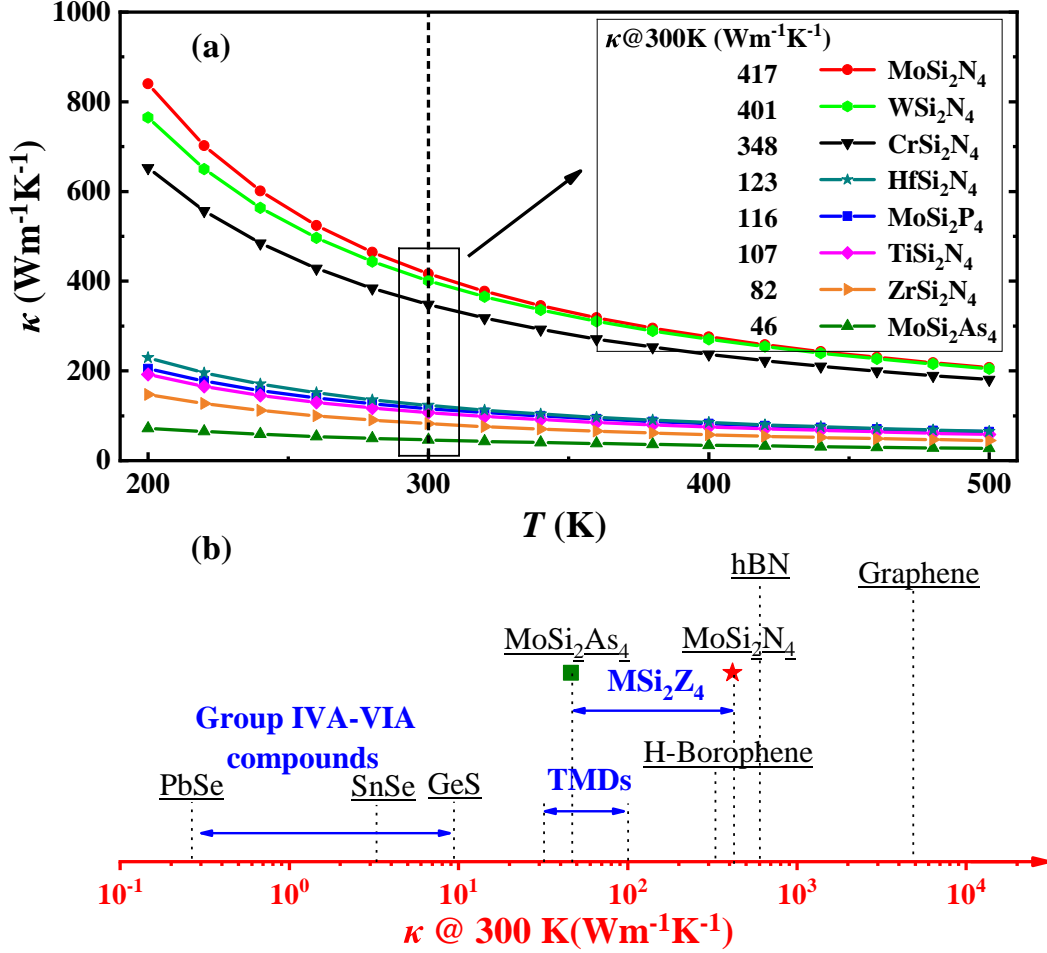


Figure 3: (a) Thermal conductivity ( $\kappa$ ) of  $\text{MA}_2\text{Z}_4$  as the function of temperature ( $T$ ), (b) the comparison of  $\kappa$  in different 2D materials at 300 K, Ref. <sup>4,11,30,32–38</sup>

large reduction of  $\kappa$  of  $\text{MoSi}_2\text{Z}_4$  could be ascribed to the following factors.

Firstly, the large reduction of  $\kappa$  with respect to Z in  $\text{MoSi}_2\text{Z}_4$  is positively related to the increasing  $\bar{m}$  and decreasing  $\Theta_D$ , as shown in Fig. 4. We also consider  $\kappa$  in the case of only changing Z-atom mass. It is found that when N mass is substituted by P mass or As mass in  $\text{MoSi}_2\text{N}_4$  (Fig. S3),  $\kappa$  is 70% or 46% of that in intrinsic  $\text{MoSi}_2\text{N}_4$ , respectively. This is much higher than that of intrinsic  $\text{MoSi}_2\text{P}_4$  (28%) and  $\text{MoSi}_2\text{As}_4$  (11%). The result elucidates that the atomic mass is not the only dominant factor.

Secondly, in phonon-dominated thermal transport, according to the Fermi's Golden rule,<sup>39,40</sup> phonon scattering processes characterized by phonon group velocity ( $v$ ) and phonon scattering rates ( $1/\tau$ ) could influence  $\kappa$ . Small  $v$  and large  $1/\tau$  mean slow and short-lifetime

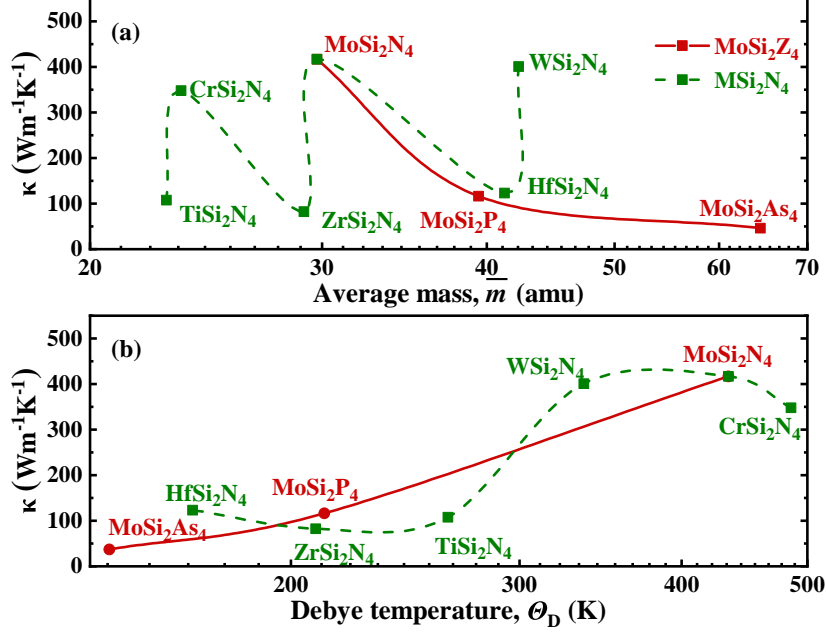


Figure 4: The room-temperature thermal conductivity of  $\text{MSi}_2\text{Z}_4$  as the function of (a) average mass  $\bar{m}$  and (b) Debye temperature  $\Theta_D$ .

phonons and thus low  $\kappa$ . Consequently, as shown in Fig. 5, the decrease in  $v$  and increase in  $1/\tau$  are demonstrably large for Z varying from N, P, to As in  $\text{MoSi}_2\text{Z}_4$ , thus leading to a large reduction in  $\kappa$ .

Thirdly, we examine the role of bond strength. From the phonon dispersion and PhDOS of the intrinsic  $\text{MoSi}_2\text{As}_4$  and  $\text{MoSi}_2\text{N}_4$  with As mass (Fig. S4), we find that the maximum phonon frequency of the former is much lower than that of the latter, and in PhDOS an obvious red shift of Si/As and Mo/Si hybrid peaks occurs in the former when compared to the latter. This indicates much weak bond between As and adjacent neighbors, which can also be verified by the calculated interatomic force constants (IFCs) in Fig. 6. Thus, the weaker Mo/Si-As bond strength substantially softens the phonon branches, and then results in stronger phonon-phonon scattering and thus quite smaller  $\kappa$ .

Fourthly, the cumulative  $\kappa$  as a function of mean free path (MFP) (Fig. S5) shows that 80% of  $\kappa$  at 300 K involves the phonons with a MFP of  $63.01 \mu\text{m}$  for  $\text{MoSi}_2\text{N}_4$ ,  $4.31 \mu\text{m}$  for  $\text{MoSi}_2\text{P}_4$ , and  $1.35 \mu\text{m}$  for  $\text{MoSi}_2\text{As}_4$ . Therefore,  $\text{MoSi}_2\text{As}_4$  possesses a MFP more than one order of magnitude smaller than that in  $\text{MoSi}_2\text{N}_4$ , also explaining its quite low  $\kappa$ .

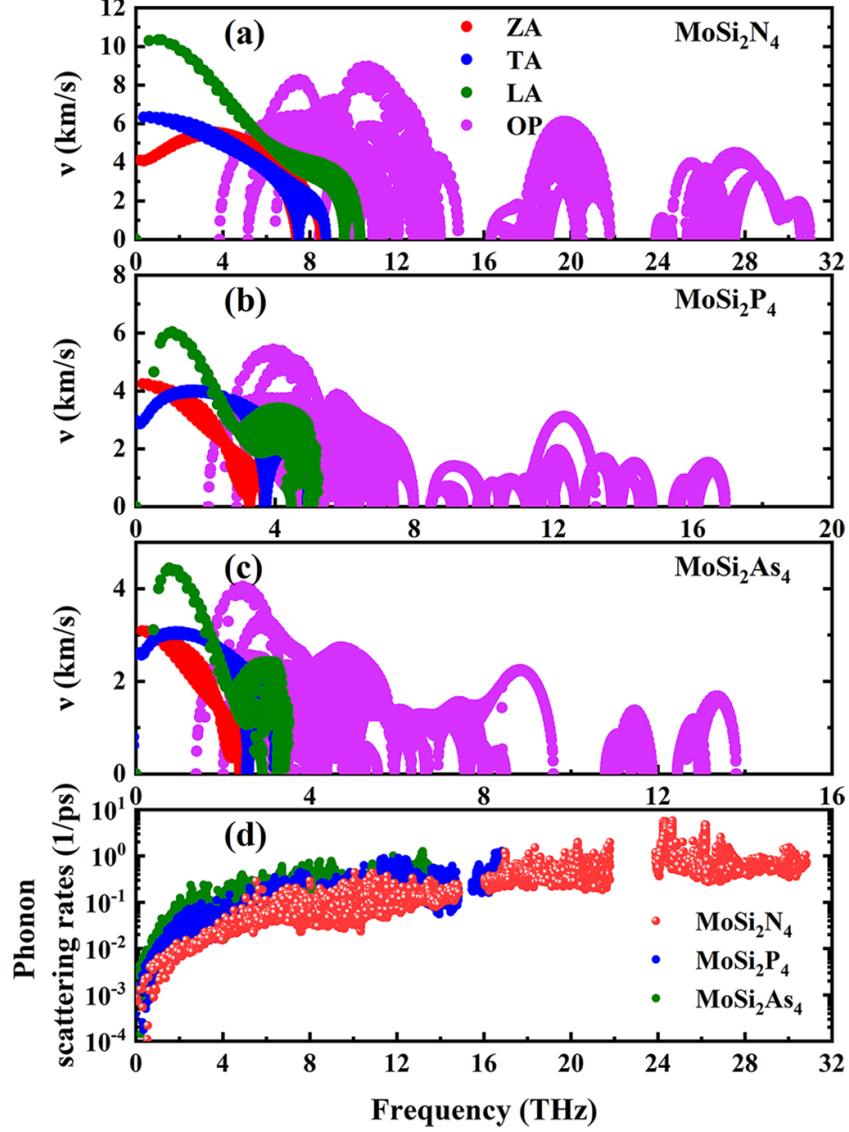


Figure 5: Phonon group velocity of (a) MoSi<sub>2</sub>N<sub>4</sub>, (b) MoSi<sub>2</sub>P<sub>4</sub> and (c) MoSi<sub>2</sub>As<sub>4</sub>, and (d) their comparison of phonon scattering rates ( $1/\tau$ ).

In short, despite of the large reduction of  $\kappa$  of MoSi<sub>2</sub>Z<sub>4</sub> when Z changes from N to P to As, it intrinsically obeys Slack's classic rule. Heavy atoms (e.g. As and P here) and weak bonds (e.g. Mo-As, Si-As here) could favor high phonon scattering rates, low Debye temperature, low phonon group velocity, and high anharmonicity, thus resulting in  $\kappa$  of MoSi<sub>2</sub>As<sub>4</sub> almost one order of magnitude smaller than that of MoSi<sub>2</sub>N<sub>4</sub>.

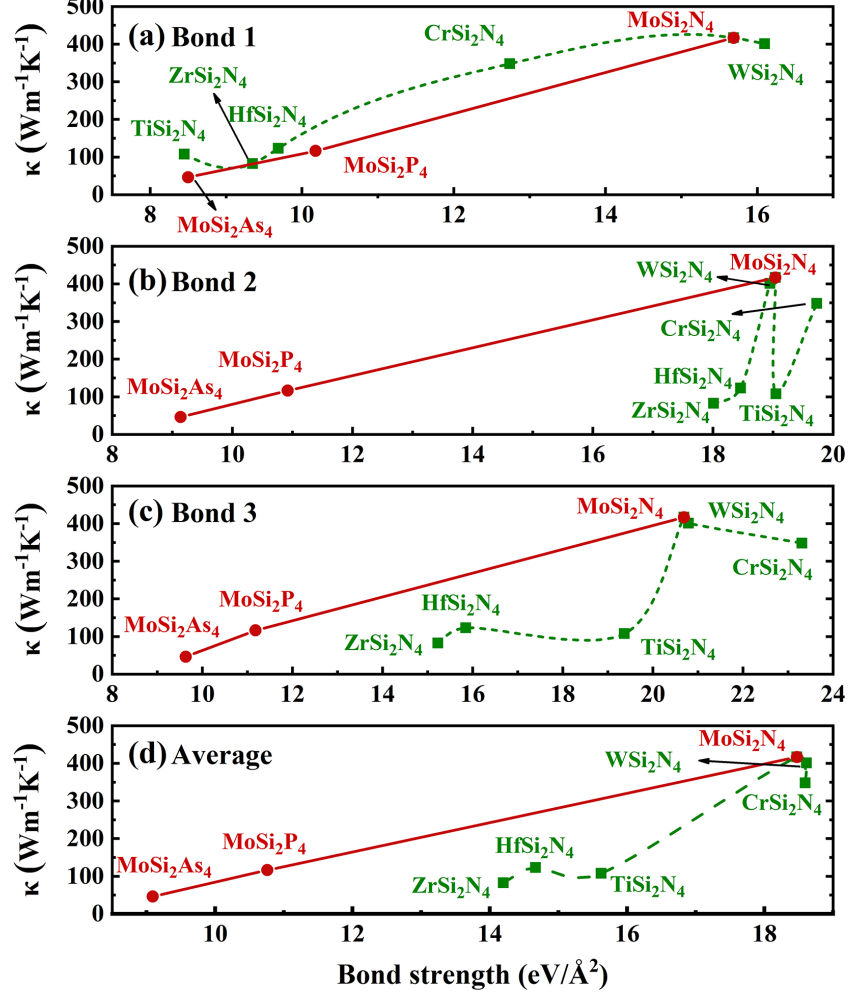


Figure 6: The room-temperature thermal conductivity of  $\text{MSi}_2\text{Z}_4$  as the function of bond strength: (a) Bond 1, (b) Bond 2, (c) Bond 3 and (d) average bond.

## 2.4. Anomalous variation of $\kappa$ in $\text{MSi}_2\text{N}_4$

In contrast to the variation of  $\kappa$  with Z in  $\text{MoSi}_2\text{Z}_4$  which follows Slack's rule, its variation with respect to M in  $\text{MSi}_2\text{N}_4$  deviates from the rule of thumb proposed by Slack.

Firstly, as shown in Fig. 4, Table 1, and Fig. S6,  $\kappa$  of  $\text{MSi}_2\text{N}_4$  does not decrease with the increasing  $\bar{m}$  (determined by M mass) and the decreasing  $\Theta_D$  and  $v$ , while an irregular oscillation occurs and no conspicuous relations exist. Secondly,  $\kappa$  of  $\text{MSi}_2\text{N}_4$  remains at the same level regardless of giant difference in M mass,  $\Theta_D$  and  $v$  when M is in the same group. For example,  $\bar{m}$  and  $\Theta_D$  in  $\text{WSi}_2\text{N}_4$  is 1.5 times as those in  $\text{CrSi}_2\text{N}_4$ , but  $\kappa$  only shows 13% difference. This indicates that  $\kappa$  of  $\text{MSi}_2\text{N}_4$  with M in the same group is insensitive to

$\bar{m}$ ,  $\Theta_D$  and  $v$ . Thirdly,  $\kappa$  of  $\text{MSi}_2\text{N}_4$  with heavier group-VIB M is around  $400 \text{ Wm}^{-1}\text{K}^{-1}$ , which is around three to four times over that with lighter group-IVB M. In other words, heavy M atoms could even result in much higher  $\kappa$ , contradictory to Slack's rule that light atoms favour high  $\kappa$ . Fourthly, in  $\text{MSi}_2\text{N}_4$  the conventional guideline that  $\Theta_D$  decreases with increasing  $\bar{m}$  holds only for M in the same group, while is invalid for M in different groups. For instance,  $\Theta_D$  of  $\text{MoSi}_2\text{N}_4$  is much higher than that of  $\text{ZrSi}_2\text{N}_4$  though their  $\bar{m}$  is very close. This could be attributed to that ZA and TA branches of  $\text{MSi}_2\text{N}_4$  with group-IVB M is much flatter than that with group-VIB M (Fig. 2). Fifthly,  $\kappa$  of  $\text{MSi}_2\text{N}_4$  does not strictly increase with the interatomic bond strength (Fig. 6), deviating from Slack's rule that stronger bonds facilitate higher  $\kappa$ . Actually, in  $\text{MSi}_2\text{N}_4$  here  $\kappa$  increases with the average bond strength (Fig. 6(d)) only when M belongs to different groups. The stronger bonds induce much higher  $\kappa$  of  $\text{MSi}_2\text{N}_4$  with group-VIB M than that with group-IVB M. However, when M is in the same group, the effect of bond strength is negligible.

In brief,  $\kappa$  varying with M in  $\text{MSi}_2\text{N}_4$  is anomalous and cannot be simply described by Slack's classic rule. In terms of M in group-IVB and -VIB as a whole,  $\kappa$  of  $\text{MSi}_2\text{N}_4$  neither increases with the decreasing  $\bar{m}$ , nor increases with the increasing  $\Theta_D$ ,  $v$  and bond strength. It depends strongly on the group of M and remains at the same level (around 100 and  $400 \text{ Wm}^{-1}\text{K}^{-1}$  for group-IVB and group-VIB M atoms, respectively) irrespective of M mass and bond strength for M in the same group.

To this end, we trace the above abnormality to fundamental vibrational properties, which are inaccessible from conventional guideline in searching for high  $\kappa$  materials. Figure 7 gives the frequency-dependent total phonon scattering rates ( $1/\tau$ ) for  $\text{MSi}_2\text{N}_4$ . It is obvious that  $1/\tau$  in  $\text{MSi}_2\text{N}_4$  with group-VIB M is much smaller than that with group-IVB M in the whole frequency range, resulting in weaker phonon scattering and thus higher  $\kappa$  of the former. When M is in the same group,  $1/\tau$  is similar and thus  $\kappa$  remains at the same level. There is anomalous phonon scattering as shown in the circle of Fig. 7. In the frequency range of 1.5–6 THz,  $1/\tau$  of  $\text{MSi}_2\text{N}_4$  with M in the same group abnormally decreases with the



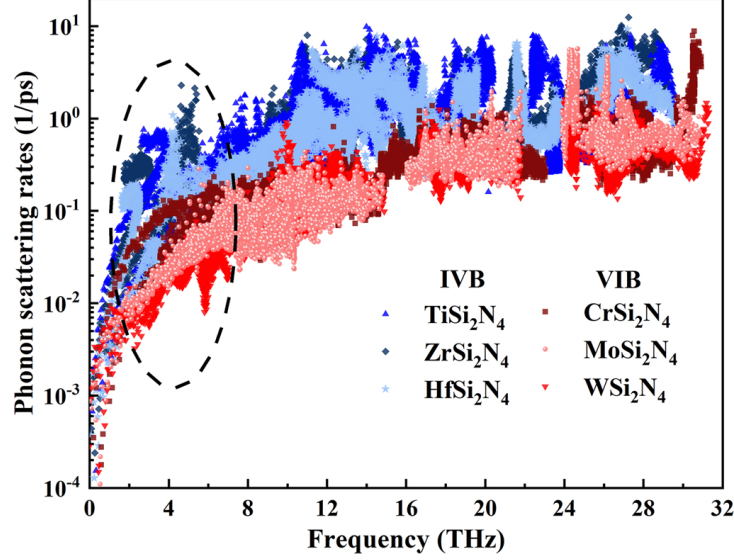


Figure 7: Total phonon scattering rates of group-IVB and -VIB  $\text{MSi}_2\text{N}_4$ .

increasing M mass. This is understandable that in Fig. S7, the phonon phase space (P3) and absolute Grüneisen parameter ( $|\gamma|$ ) approximately decrease with the increasing M mass, which indicates the reduced phonon scattering channels, weak scattering strengths, and thus higher  $\kappa$ .

The contribution of each phonon branch to the total  $\kappa$  is shown in Table 2. One can find that the acoustic branches dominate  $\kappa$  of  $\text{MSi}_2\text{N}_4$ , whose contribution is 74–84%. Besides, the lowest five optical branches contribute 14–25%. LA branch contributes more in the case of group-VIB M, while TA branch dominates in the case of group-IVB M.

For more detailed evaluation, we examine the three-phonon scattering channels involving three acoustic phonons (AAA), two acoustic phonons combining with one optical phonon (AAO), and one acoustic phonon combining with two optical phonons (AOO), as shown in Fig. 8. For each scattering channel, the scattering process is found much weaker in group-VIB M than group-IVB M. This is intrinsically attributed to the interplay of certain basic properties such as bunching/flatness of acoustic/optical branches, frequency gap between acoustic and optical phonons (a-o gap), etc.<sup>41,42</sup> It is apparent in Fig. 2 that the acoustic branches in  $\text{MSi}_2\text{N}_4$  with group-VIB M are more bunched and less flattened than those in  $\text{MSi}_2\text{N}_4$  with group-IVB M. In addition, the lowest six optical branches close to acoustic

Table 2: Calculated  $\kappa$  contributions from different phonon branches. OP (low) indicates the first six low-frequency optical branches.

	Thermal Contribution (%)				
	ZA	TA	LA	OP (total)	OP (low)
CrSi <sub>2</sub> N <sub>4</sub>	8.7	37.7	35.8	17.8	16.8
MoSi <sub>2</sub> N <sub>4</sub>	21.7	20.6	34.5	23.2	22.2
WSi <sub>2</sub> N <sub>4</sub>	18.6	22.1	33.4	25.9	24.9
TiSi <sub>2</sub> N <sub>4</sub>	8.2	57.3	15.3	19.2	16.1
ZrSi <sub>2</sub> N <sub>4</sub>	14.3	45.5	23.9	16.3	13.8
HfSi <sub>2</sub> N <sub>4</sub>	11.7	46.0	25.8	16.5	14.2

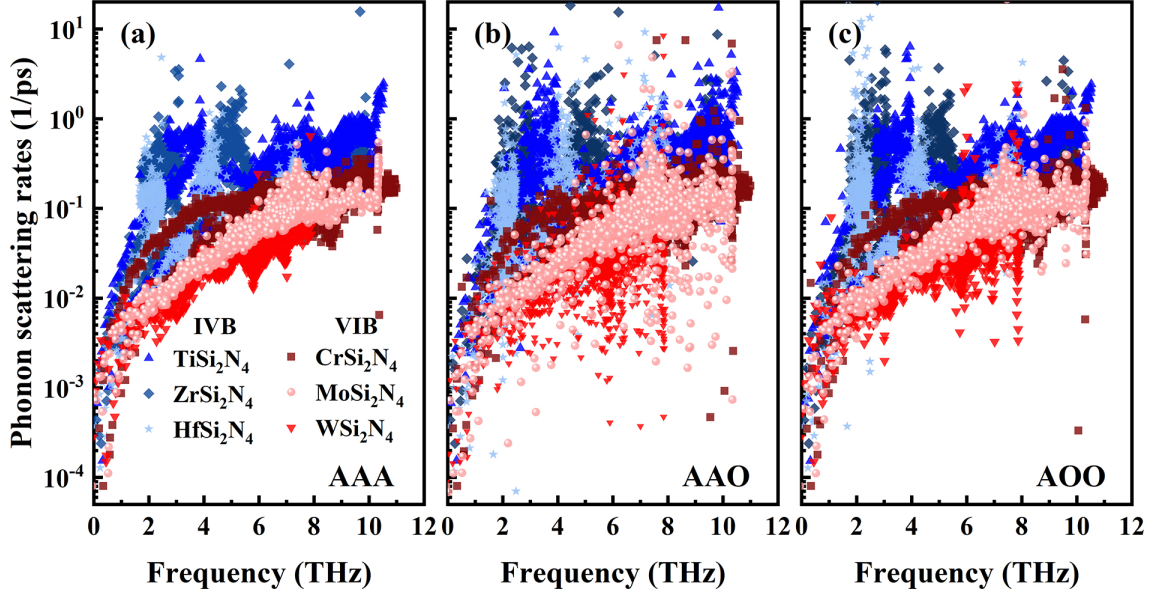


Figure 8: Phonon scattering rates of MSi<sub>2</sub>N<sub>4</sub> for particular interacting channels: (a) AAA, (b) AAO and (c) AOO.

branches are also more bunched in MSi<sub>2</sub>N<sub>4</sub> with group-VIB M. These give weaker AAA, AAO, and AOO scattering and thus high  $\kappa$  of MSi<sub>2</sub>N<sub>4</sub> with group-VIB M. In MSi<sub>2</sub>N<sub>4</sub> with M in the same group, the slight difference in the combination of these phonon features contributes to the subtle difference in  $\kappa$ .

The phonon scattering rates for different scattering channels also exhibit abnormality

with respect to  $\overline{m}$ , as shown in Fig. S8. For instance,  $\overline{m}$  of  $\text{MoSi}_2\text{N}_4$  is close to that of  $\text{ZrSi}_2\text{N}_4$ , but the rates for all the AAA, AAO, and AOO scattering in  $\text{MoSi}_2\text{N}_4$  is one order of magnitude lower than that in  $\text{ZrSi}_2\text{N}_4$ , leading to  $\kappa$  of  $\text{ZrSi}_2\text{N}_4$  is only 20% of that of  $\text{MoSi}_2\text{N}_4$ . Though  $\overline{m}$  of  $\text{WSi}_2\text{N}_4$  is two times of that of  $\text{TiSi}_2\text{N}_4$ ,  $\kappa$  of the former are nearly four times of that of the latter due to the much lower rates for AAA, AAO and AOO scattering in  $\text{WSi}_2\text{N}_4$ .

### 3. CONCLUSIONS

In summary, we apply density functional theory and phonon Boltzmann transport equation to calculate the  $\kappa$  of eight types of 2D  $\text{MSi}_2\text{Z}_4$  semiconductors ( $\text{M} = \text{Mo}, \text{Cr}, \text{W}, \text{Ti}, \text{Zr}, \text{Hf}$  and  $\text{Z} = \text{N}, \text{P}, \text{As}$ ) and deliver the fundamental understanding of  $\kappa$ . The main conclusions are summarized in the following.

1) 2D semiconductors  $\text{MoSi}_2\text{N}_4$  and  $\text{WSi}_2\text{N}_4$  are found to possess a high  $\kappa$  over  $400 \text{ Wm}^{-1}\text{K}^{-1}$ , comparable to that of the good thermal conductor copper.

2) In  $\text{MoSi}_2\text{Z}_4$ ,  $\kappa$  significantly decreases by one order of magnitude from  $\text{Z} = \text{N}$  to  $\text{Z} = \text{As}$ . The variation of  $\kappa$  with  $\text{Z}$  complies with Slack's classic rule. Heavy atoms (e.g. As) and weak bonds (e.g. Mo-As, Si-As) could favor high phonon scattering rates, low Debye temperature, low phonon group velocity, and high anharmonicity and thus low  $\kappa$ .

3) When  $\text{M}$  is in the same group,  $\kappa$  of  $\text{MSi}_2\text{N}_4$  varying with  $\text{M}$  is anomalous and deviates from Slack's classic rule. It is insensitive to  $\overline{m}$ ,  $\Theta_{\text{D}}$ ,  $v$ , and bond strength owing to the similar phonon scattering properties.

4) When  $\text{M}$  is in different group,  $\kappa$  of  $\text{MSi}_2\text{N}_4$  with group-VIB  $\text{M}$  is three to four times large as that with group-IVB  $\text{M}$  in spite of  $\text{M}$  mass, due to that the phonon scattering rates of former are nearly one order of magnitude lower than that of the latter. This could be intrinsically ascribed to the much higher bond strength of  $\text{M-N}$  bonds and exterior  $\text{Si-N}$  bonds in  $\text{MSi}_2\text{N}_4$  with group-VIB  $\text{M}$ .

5) Although  $\kappa$  variation in  $\text{MSi}_2\text{N}_4$  with respect to M as a whole is anomalous and cannot be well described by Slack’s rule of thumb, it could be traced to an interplay of certain basic vibrational properties that lie outside of the conventional guidelines. The acoustic branches are more bunched and less flattened, and their nearby six optical branches are more bunched in  $\text{MSi}_2\text{N}_4$  with group-VIB M than in  $\text{MSi}_2\text{N}_4$  with group-IVB M, giving weaker AAA, AAO, and AOO scattering and thus higher  $\kappa$  of the former. In  $\text{MSi}_2\text{N}_4$  with M in the same group, the slight difference in these phonon features, i.e. bunching strength and flatness of acoustic branches and their nearby optical branches, contributes to the subtle difference in  $\kappa$ .

In this work, it has been identified that 2D semiconductor  $\text{MSi}_2\text{N}_4$  with group-VIB M possesses high  $\kappa$  which could open new opportunities for heat dissipation and thermal management in semiconductor device. The anomalous variation of  $\kappa$  in  $\text{MSi}_2\text{Z}_4$  has been clarified as well. Since  $\text{MSi}_2\text{Z}_4$  is the multi-layered 2D structure compared with other materials (e.g. graphene, silicene, BP, h-BN, TMDs etc.), the work has also given important insights into analyzing the physics of  $\kappa$  in layered 2D systems.

## 4. METHODOLOGY SECTION

The first-principles calculations are performed based on density functional theory (DFT),<sup>43</sup> as implemented in the Vienna *ab initio* simulation package (VASP).<sup>44,45</sup> The generalized gradient approximation (GGA) functional within Perdew-Burke-Ernzerhof (PBE) form is applied for the exchange-correlation functional,<sup>46</sup> and the projector-augmented-wavepotential (PAW) is used to describe the electron-ion interactions.<sup>47</sup> The convergence criteria for energies and forces are  $10^{-7}$  eV and  $10^{-4}$  eV/Å, respectively. A cutoff energy of 500 eV and  $15 \times 15 \times 1$  Monkhorst-Pack  $k$ -mesh in the first Brillouin zone are adopted. A vacuum layer of 20 Å is used to eliminate the interaction between layers.

Electron localization function (ELF) of  $\text{MSi}_2\text{Z}_4$  is considered, as shown in Fig. S9. The maximum ELF value between the two atoms of each bond is above 0.85, indicating interstitial

strong localization of electrons and thus a covalent-like nature of these bonds. Considering the polarization effect of group-IVB and -VIB transition metal atoms on phononic nature and further thermal transport properties, we also calculate Born effective charges and dielectric constant, listed in Table S2. Phonon dispersion and harmonic (2<sup>nd</sup>) interatomic force constants (IFCs) are calculated via finite displacement method within PHONOPY package.<sup>48</sup> The comparison of phonon dispersion of MoSi<sub>2</sub>N<sub>4</sub> with or without polarization is shown in Fig. S10. It is worth noting that, the high-frequency optical branches show obvious splitting near  $\Gamma$  point which indicates the strong polarization phenomenon. Thus, Born effective charges and dielectric constant should be considered in calculations of phonon dispersion and thermal conductivity. The supercell of  $5 \times 5 \times 1$  and  $k$ -mesh of  $5 \times 5 \times 1$  are adopted. The anharmonic (3<sup>rd</sup>) IFCs are obtained by the same supercell and  $k$ -mesh. Then,  $\kappa$  and phonon scattering mechanism are obtained by solving phonon Boltzmann transport equation (BTE).<sup>49,50</sup> The calculating process is performed by ShengBTE package with a  $q$ -mesh of  $81 \times 81 \times 1$  and a cutoff distance of 0.5 nm. The convergence of  $\kappa$  against  $q$ -mesh is tested from  $61 \times 61 \times 1$  to  $101 \times 101 \times 1$  as shown in Figure S11.

Lattice thermal conductivity tensor ( $\kappa_{\alpha\beta}$ ) at different temperature ( $T$ ) can be expressed as:<sup>50</sup>

$$\kappa_{\alpha\beta} = \frac{1}{k_B T^2 N V} \sum_{\lambda} (\hbar \omega_{\lambda}) f_{\lambda}^0 (1 + f_{\lambda}^0) \nu_{\lambda}^{\alpha} F_{\lambda}^{\beta} \quad (1)$$

where  $k_B$ ,  $\hbar$  and  $f_{\lambda}^0$  are Boltzmann constant, reduced Planck constant and equilibrium Bose-Einstein distribution function, respectively.  $V$  is the volume of unit cell.  $\lambda$  denotes a phonon branch characterized by the wave vector  $q$  points.  $N$  is the number of  $q$  points in the Brillouin zone.  $\omega_{\lambda}$  and  $\nu_{\lambda}$  are the angular frequency and phonon group velocity.  $F_{\lambda}^{\beta}$  is defined as:<sup>51</sup>

$$F_{\beta}^{\lambda} = \tau_{\lambda}^0 (\nu_{\lambda}^{\beta} + \Delta_{\lambda}^{\beta}) \quad (2)$$

in which  $\tau_{\lambda}^0$  is phonon relaxation time from single-mode relaxation time approximation and

$\Delta_\lambda^\beta$  is the correction term from iterative solution of BTE to modify the error.

In insulating and semiconductor materials, heat is mainly transported by lattice vibration.<sup>52</sup> Here the thermal transport properties of the 2D semiconductor  $\text{MSi}_2\text{Z}_4$  system are considered, and three-phonon scattering mechanism which contains phonon-phonon (pp) diffusion and isotope effect (iso) is discussed. The phonon relaxation time can be expressed as:

$$\frac{1}{\tau_\lambda^0} = \frac{1}{\tau_\lambda^{\text{pp}}} + \frac{1}{\tau_\lambda^{\text{iso}}} \quad (3)$$

Debye temperature is a single parameter to describe the temperature-dependent heat capacity in conventional Debye model.<sup>53</sup> It depends on the dispersion law of acoustic phonons, and the average Debye temperature ( $\Theta_D$ ) is expressed as:<sup>4,54</sup>

$$\frac{1}{\Theta_D^3} = \frac{1}{3} \left( \frac{1}{\Theta_{\text{ZA}}^3} + \frac{1}{\Theta_{\text{TA}}^3} + \frac{1}{\Theta_{\text{LA}}^3} \right) \quad (4)$$

and  $\Theta_i$  ( $i = \text{ZA}, \text{TA}, \text{LA}$ ) is defined as

$$\Theta_i = \frac{\hbar\omega_i}{k_B} \quad (5)$$

where  $\omega_i$  is the maximum frequency of  $i^{\text{th}}$  acoustic branch.

## ACKNOWLEDGMENT

The authors acknowledge the support from 15<sup>th</sup> Thousand Youth Talents Program of China, the National Natural Science Foundation of China (NSFC 11902150), the Research Fund of State Key Laboratory of Mechanics and Control of Mechanical Structures (MCMS-I-0419G01, MCMS-I-0421K01), the Fundamental Research Funds for the Central Universities, the open project of National Laboratory of Solid State Microstructures (M34055) and a project Funded by the Priority Academic Program Development of Jiangsu Higher Education Institutions.

# AUTHOR INFORMATION

## Corresponding Author

**Min Yi** – Institute for Frontier Science, Institute of Nanoscience, State Key Lab of Mechanics and Control of Mechanical Structures & Key Lab for Intelligent Nano Materials and Devices of Ministry of Education & College of Aerospace Engineering, Nanjing University of Aeronautics and Astronautics (NUAA), Nanjing 210016, China; National Laboratory of Solid State Microstructures, Nanjing University, Nanjing 210093, China;

Email: yimin@nuaa.edu.cn

**Wanlin Guo** – Institute for Frontier Science, Institute of Nanoscience, State Key Lab of Mechanics and Control of Mechanical Structures & Key Lab for Intelligent Nano Materials and Devices of Ministry of Education & College of Aerospace Engineering, Nanjing University of Aeronautics and Astronautics (NUAA), Nanjing 210016, China;

Email: wlguo@nuaa.edu.cn

## Author

**Yan Yin** – Institute for Frontier Science, Institute of Nanoscience, State Key Lab of Mechanics and Control of Mechanical Structures & Key Lab for Intelligent Nano Materials and Devices of Ministry of Education & College of Aerospace Engineering, Nanjing University of Aeronautics and Astronautics (NUAA), Nanjing 210016, China;

Email: yanyin0330@nuaa.edu.cn

# SUPPORTING INFORMATION

Electronic band structures and phonon density of states of  $\text{MSi}_2\text{Z}_4$  (Figure S1 and S2); the effect of mass and bond strength induced by Z atom on the thermal conductivity ( $\kappa$ ) of  $\text{MoSi}_2\text{Z}_4$  (Figure S3 and S4); the normalized cumulative thermal conductivity versus mean free path of  $\text{MSi}_2\text{Z}_4$  (Figure S5); phonon group velocity, room-temperature  $\kappa$ , phase space and absolute Grüneisen parameter versus frequency of  $\text{MSi}_2\text{N}_4$  (Figure S6 and S7); phonon

scattering rates for particular interacting channels (Figure S8); electron localization function (ELF) distribution of  $\text{MSi}_2\text{Z}_4$  in the (110) plane (Figure S9); phonon dispersion spectrum of  $\text{MoSi}_2\text{N}_4$  with or without polarization effect (Figure S10); convergence test of grid density of  $\kappa$  (Figure S11); band gaps of 2D  $\text{MSi}_2\text{Z}_4$  by GGA and HSE (Table S1); born effective charges and dielectric constants of 2D  $\text{MSi}_2\text{Z}_4$  (Table S2)

## References

- (1) Koenig, S. P.; Doganov, R. A.; Schmidt, H.; Castro Neto, A. H.; Özyilmaz, B. Electric Field Effect in Ultrathin Black Phosphorus. Appl. Phys. Lett. **2014**, 104, 103106.
- (2) Gu, X.; Yang, R. Phonon Transport in Single-layer Transition Metal Dichalcogenides: A First-principles Study. Appl. Phys. Lett. **2014**, 105, 131903.
- (3) Qin, G.; Qin, Z.; Fang, W.; Zhang, L.; Yue, S.; Yan, Q.; Hu, M.; Su, G. Diverse Anisotropy of Phonon Transport in Two-dimensional Group IV - VI Compounds: A Comparative Study. Nanoscale **2016**, 8, 11306–11319.
- (4) Liu, P.; Bo, T.; Xu, J.; Yin, W.; Zhang, J.; Wang, F.; Eriksson, O.; Wang, B. T. First-principles Calculations of the Ultralow Thermal Conductivity in Two-dimensional Group-IV Selenides. Phys. Rev. B **2018**, 98, 235426.
- (5) Taube, A.; Judek, J.; Łapińska, A.; Zdrojek, M. Temperature-dependent Thermal Properties of Supported  $\text{MoS}_2$  Monolayers. ACS Appl. Mater. Inter. **2015**, 7, 5061–5065.
- (6) Zhang, X.; Sun, D.; Li, Y.; Lee, G.; Cui, X.; Chenet, D.; You, Y.; Heinz, T. F.; Hone, J. C. Measurement of Lateral and Interfacial Thermal Conductivity of Single- and Bilayer  $\text{MoS}_2$  and  $\text{MoSe}_2$  Using Refined Optothermal Raman Technique. ACS Appl. Mater. Inter. **2015**, 7, 25923–25929.
- (7) Zhao, L.; Lo, S.; Zhang, Y.; Sun, H.; Tan, G.; Uher, C.; Wolverton, C.; Dravid, V. P.;



- Kanatidis, M. G. Ultralow Thermal Conductivity and High Thermoelectric Figure of Merit in SnSe Crystals. Nature **2014**, 508, 373–377.
- (8) Saito, Y.; Iizuka, T.; Koretsune, T.; Arita, R.; Shimizu, S.; Iwasa, Y. Gate-Tuned Thermoelectric Power in Black Phosphorus. Nano Lett. **2016**, 16, 4819–4824.
- (9) Li, L.; Yu, Y.; Ye, G. J.; Ge, Q.; Ou, X.; Wu, H.; Feng, D.; Chen, X. H.; Zhang, Y. Black Phosphorus Field-effect Transistors. Nat. Nanotechnol. **2014**, 9, 372–377.
- (10) Zhang, Z.; Xie, Y.; Ouyang, Y.; Chen, Y. A Systematic Investigation of Thermal Conductivities of Transition Metal Dichalcogenides. Int. J. Heat Mass Tran. **2017**, 108, 417–422.
- (11) Balandin, A. A.; Ghosh, S.; Bao, W.; Calizo, I.; Lau, C. Superior Thermal Conductivity of Single-layer Graphene. Nano Lett. **2008**, 8, 902–907.
- (12) Fan, H.; Wu, H.; Lindsay, L.; Hu, Y. Ab Initio Investigation of Single-layer High Thermal Conductivity Boron Compounds. Phys. Rev. B **2019**, 100, 085420.
- (13) Hong, Y.; Zhang, J.; Zeng, X. Monolayer and Bilayer Polyaniline C<sub>3</sub>N: Two-dimensional Semiconductors With High Thermal Conductivity. Nanoscale **2018**, 10, 4301–4310.
- (14) Dong, Y.; Zhang, C.; Meng, M.; Groves, M. M.; Lin, J. Novel Two-dimensional Diamond Like Carbon Nitrides with Extraordinary Elasticity and Thermal Conductivity. Carbon **2018**, 138, 319–324.
- (15) Mortazavi, B.; Shahrokhi, M.; Raeisi, M.; Zhuang, X.; Pereira, L. F. C.; Rabczuk, T. Outstanding Strength, Optical Characteristics and Thermal Conductivity of Graphene-like BC<sub>3</sub> and BC<sub>6</sub>N Semiconductors. Carbon **2019**, 149, 733–742.
- (16) Hu, Y.; Li, D.; Yin, Y.; Li, S.; Ding, G.; Zhou, H.; Zhang, G. The Important Role of Strain on Phonon Hydrodynamics in Diamond-like Bi-layer Graphene. Nanotechnology **2020**, 31, 335711.

- (17) Hong, Y.; Liu, Z.; Wang, L.; Zhou, T.; Ren, W. Chemical Vapor Deposition of Layered Two-dimensional  $\text{MoSi}_2\text{N}_4$  Materials. Science **2020**, 369, 670–674.
- (18) Wang, L.; Shi, Y.; Liu, M.; Hong, Y.; Chen, M.; Li, R.; Gao, Q.; Ren, W.; Cheng, H.; Li, Y.; Chen, X. Intercalated Architecture of  $\text{MA}_2\text{Z}_4$  Family Layered Van Der Waals Materials with Emerging Topological, Magnetic and Superconducting Properties. Nat. Commun. **2021**, 12, 1–10.
- (19) Mortazavi, B.; Javvaji, B.; Shojaei, F.; Rabczuk, T.; V., S. A.; Zhuang, X. Exceptional Piezoelectricity, High Thermal Conductivity and Stiffness and Promising Photocatalysis in Two-dimensional  $\text{MoSi}_2\text{N}_4$  Family Confirmed by First-principles. Nano Energy **2021**, 82, 105716.
- (20) Li, S.; Wu, W.; Feng, X.; Guan, S.; Feng, W.; Yao, Y.; Yang, S. A. Valley-dependent Properties of Monolayer  $\text{MoSi}_2\text{N}_4$ ,  $\text{WSi}_2\text{N}_4$ , and  $\text{MoSi}_2\text{As}_4$ . Phys. Rev. B **2020**, 102, 235435.
- (21) Yang, C.; Song, Z.; Sun, X.; Lu, J. Valley Pseudospin in Monolayer  $\text{MoSi}_2\text{N}_4$  and  $\text{MoSi}_2\text{As}_4$ . Phys. Rev. B **2021**, 103, 035308.
- (22) Zhong, H.; Xiong, W.; Lv, P.; Yu, J.; Yuan, S. Strain-induced Semiconductor to Metal Transition in  $\text{MA}_2\text{Z}_4$  Bilayers ( $\text{M}=\text{Ti}, \text{Cr}, \text{Mo}$ ;  $\text{A}=\text{Si}$ ;  $\text{Z}=\text{N}, \text{P}$ ). Phys. Rev. B **2021**, 103, 085124.
- (23) Cao, L.; Zhou, G.; Wang, Q.; Ang, L. K.; Ang, Y. S. Two-dimensional Van Der Waals Electrical Contact to Monolayer  $\text{MoSi}_2\text{N}_4$ . Appl. Phys. Lett. **2021**, 118, 013106.
- (24) Chen, J.; Tang, Q. The Versatile Electronic, Magnetic and Photo-Electro Catalytic Activity of a New 2D  $\text{MA}_2\text{Z}_4$  Family. Chem. Eur. J. **2021**, 27, 1–10.
- (25) Yang, J.; Zhao, L.; Li, S.; Liu, H.; Wang, L.; Chen, M.; Gao, J.; Zhao, J. Accurate

- Electronic Properties and Non-linear Optical Response of Two-dimensional  $\text{MA}_2\text{Z}_4$ . Nanoscale **2021**, 13, 5479–5488.
- (26) Yu, J.; Zhou, J.; Wan, X.; Li, Q. High Intrinsic Lattice Thermal Conductivity in Monolayer  $\text{MoSi}_2\text{N}_4$ . New J. Phys. **2021**, 23, 033005.
- (27) Slack, G. A. Anisotropic Thermal Conductivity of Pyrolytic Graphite. Phys. Rev. **1962**, 127, 694–701.
- (28) Slack, G. A. Nonmetallic Crystals with High Thermal Conductivity. J. Phys. Chem. Solids **1973**, 34, 321–335.
- (29) Hu, Y.; Yin, Y.; Ding, G.; Liu, J.; Zhou, H.; Feng, W.; Zhang, G.; Li, D. High Thermal Conductivity in Covalently Bonded Bi-layer Honeycomb Boron Arsenide. Mater. Today Phys. **2021**, 17, 100346.
- (30) Li, T.; Nie, G.; Sun, Q. Highly Sensitive Tuning of Lattice Thermal Conductivity of Graphene-like Borophene by Fluorination and Chlorination. Nano Res. **2020**, 13, 1171–1177.
- (31) Li, J.; Liu, P. F.; Zhang, C.; Shi, X.; Jiang, S.; Chen, W.; Yin, H.; Wang, B. T. Lattice Vibrational Modes and Phonon Thermal Conductivity of Single-layer  $\text{GaGeTe}$ . Journal of Materiomics **2020**, 6, 723–728.
- (32) Cai, Y.; Lan, J.; Zhang, G.; Zhang, Y. Lattice Vibrational Modes and Phonon Thermal Conductivity of Monolayer  $\text{MoS}_2$ . Phys. Rev. B **2014**, 89, 035438.
- (33) Gu, X.; Yang, R. Phonon Transport in Single-layer Transition Metal Dichalcogenides: A First-principles Study. Appl. Phys. Letters. **2014**, 105, 131903.
- (34) Torres, P.; Alvarez, F. X.; Cartoixa X. ; Rurali, R. Thermal Conductivity and Phonon Hydrodynamics in Transition Metal Dichalcogenides from First-principles. 2D Mater. **2019**, 6, 035002.

- (35) Sun, Y.; Shuai, Z.; Wang, D. Reducing Lattice Thermal Conductivity of the Thermoelectric SnSe Monolayer: Role of Phonon–electron Coupling. J. Phys. Chem. C **2019**, 123, 12001–12006.
- (36) Ghosh, S.; Calizo, I.; Teweldebrhan, D.; Pokatilov, E. P.; Nika, D.; Balandin, A. A.; Bao, W.; Miao, F.; Lau, C. N. Extremely High Thermal Conductivity of Graphene: Prospects for Thermal Management Applications in Nanoelectronic Circuits. Appl. Phys. Lett. **2008**, 92, 1148.
- (37) Hong, Y.; Zhang, J.; Zeng, X. Monolayer and Bilayer Polyaniline C<sub>3</sub>N: Two-dimensional Semiconductors with High Thermal Conductivity. Nanoscale **2018**, 10, 4301–4310.
- (38) Lindsay, L.; Broido, D. A. Enhanced Thermal Conductivity and Isotope Effect in Single-layer Hexagonal Boron Nitride. Phys. Rev. B **2011**, 84, 155421–155421.
- (39) Lindsay, L.; Broido, D. A.; Mingo, N. Lattice Thermal Conductivity of Single-walled Carbon Nanotubes: Beyond the Relaxation Time Approximation and Phonon-phonon Scattering Selection Rules. Phys. Rev. B **2009**, 80, 125407.
- (40) Tong, Z.; Li, S.; Ruan, X.; Bao, H. Comprehensive First-principles Analysis of Phonon Thermal Conductivity and Electron-phonon Coupling in Different Metals. Phys. Rev. B **2019**, 100, 144306.
- (41) Lindsay, L.; Broido, D. A.; Reinecke, T. L. Thermal Conductivity and Large Isotope Effect in GaN from First Principles. Phys. Rev. Lett. **2012**, 109, 095901.
- (42) Lindsay, L.; Broido, D. A.; Reinecke, T. L. First-Principles Determination of Ultrahigh Thermal Conductivity of Boron Arsenide: A Competitor for Diamond? Phys. Rev. Lett. **2013**, 111, 025901.
- (43) Kohn, W.; Sham, L. J. Self-Consistent Equations Including Exchange and Correlation Effects. Phys. Rev. **1965**, 140, A1133.

- (44) Hafner, J. Materials Simulations using VASP-A Quantum Perspective to Materials Science. Comput. Phys. Commun. **2007**, 177, 6–13.
- (45) Hafner, J. Ab-Initio Simulations of Materials Using VASP: Density-functional Theory and Beyond JÜRGEN. J. Comput. Chem. **2008**, 29, 2044–2078.
- (46) Kresse, G. G.; Furthmüller, J. Efficient Iterative Schemes for Ab Initio Total-energy Calculations Using a Plane-wave Basis Set. Phys. Rev. B **1996**, 54, 11169.
- (47) Blöchl, P. E. Projector Augmented-wave Method. Phys. Rev. B **1994**, 50, 17953–17979.
- (48) Togo, A.; Tanaka, I. First Principles Phonon Calculations in Materials Science. Scripta. Mater. **2015**, 108, 1–5.
- (49) Chernatynskiy, A.; Phillpot, S. R. Evaluation of Computational Techniques for Solving the Boltzmann Transport Equation for Lattice Thermal Conductivity Calculations. Phys. Rev. B **2010**, 82, 1456–1461.
- (50) Li, W.; Carrete, J.; A. Katcho, N.; Mingo, N. ShengBTE: A Solver of the Boltzmann Transport Equation for Phonons. Comput. Phys. Commun. **2014**, 185, 1747–1758.
- (51) Ward, A.; Broido, D. A.; Stewart, D. A.; Deinzer, G. Ab Initio Theory of the Lattice Thermal Conductivity in Diamond. Phys. Rev. B **2009**, 80, 125203.
- (52) Zhou, Y.; Fan, Z.; Qin, G.; Yang, J.; Ouyang, T.; Hu, M. Methodology Perspective of Computing Thermal Transport in Low-dimensional Materials and Nanostructures : The Old and the New. ACS Omega **2018**, 3, 3278–3284.
- (53) Asen-Palmer, M.; Bartkowski, K.; Gmelin, E.; Cardona, M.; Zhernov, A. P.; Inyushkin, A. V.; Taldenkov, A.; Ozhogin, V. I.; Itoh, K. M.; Haller, E. E. Thermal Conductivity of Germanium Crystals with Different Isotopic Compositions. Phys. Rev. B **1997**, 56, 9431–9447.

- (54) Zhang, Y. First-principles Debye–Callaway Approach to Lattice Thermal Conductivity. J. Materiomics **2016**, 2, 237–247.

Supporting information

High and anomalous thermal conductivity in mono-  
layer  $\text{MSi}_2\text{Z}_4$  semiconductors

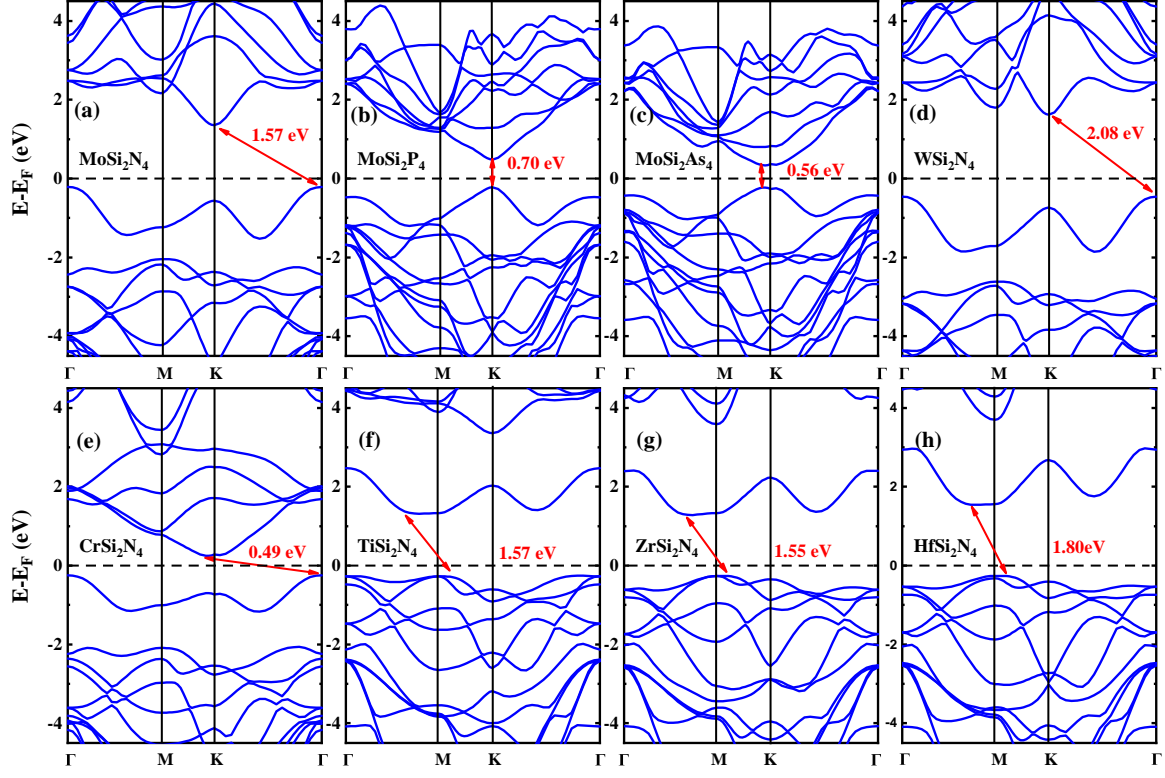


Figure S1. Electronic band structures of  $\text{MSi}_2\text{Z}_4$ : (a)  $\text{MoSi}_2\text{N}_4$ , (b)  $\text{MoSi}_2\text{P}_4$ , (c)  $\text{MoSi}_2\text{As}_4$ , (d)  $\text{WSi}_2\text{N}_4$ , (e)  $\text{CrSi}_2\text{N}_4$ , (f)  $\text{TiSi}_2\text{N}_4$ , (g)  $\text{ZrSi}_2\text{N}_4$  and (h)  $\text{HfSi}_2\text{N}_4$ .

Table S1. Band gaps of 2D  $\text{MSi}_2\text{Z}_4$  by GGA and HSE, respectively.

	$\text{MoSi}_2\text{N}_4$	$\text{MoSi}_2\text{P}_4$	$\text{MoSi}_2\text{As}_4$	$\text{WSi}_2\text{N}_4$	$\text{CrSi}_2\text{N}_4$	$\text{TiSi}_2\text{N}_4$	$\text{ZrSi}_2\text{N}_4$	$\text{HfSi}_2\text{N}_4$
GGA (eV)	1.56	0.70	0.56	2.08	0.49	1.57	1.55	1.80
HSE (eV)	2.40	1.11	0.98	2.64	1.11	2.50	2.41	2.70



Table S2. Born effective charges ( $Z^*$ ) of each nonequivalent atom (M, Si, Z1, Z2) and dielectric constants ( $\epsilon$ ) of 2D  $\text{MSi}_2\text{Z}_4$ .

	component	$Z^*$ (M)	$Z^*$ (Si)	$Z^*$ (Z1)	$Z^*$ (Z2)	$\epsilon$
$\text{MoSi}_2\text{N}_4$	xx	0.88	3.30	-0.84	-2.90	5.14
	yy	0.88	3.30	-0.85	-2.90	5.14
	zz	-0.02	1.03	-0.48	-0.53	1.65
$\text{MoSi}_2\text{P}_4$	xx	-3.74	1.81	1.84	-1.78	10.82
	yy	-3.74	1.81	1.84	-1.78	10.82
	zz	-0.59	0.28	0.28	-0.11	2.27
$\text{MoSi}_2\text{As}_4$	xx	-4.15	1.49	2.12	-1.53	12.76
	yy	-4.15	1.49	2.12	-1.53	12.76
	zz	-0.58	0.18	0.17	-0.06	2.49
$\text{WSi}_2\text{N}_4$	xx	1.39	3.31	-1.16	-2.85	4.66
	yy	1.39	3.31	-1.16	-2.85	4.66
	zz	-0.02	0.97	-0.64	-0.33	1.64
$\text{CrSi}_2\text{N}_4$	xx	-0.58	3.21	-0.03	-2.89	6.59
	yy	-0.58	3.21	-0.03	-2.89	6.59
	zz	-0.10	0.91	-0.38	-0.47	1.64
$\text{TiSi}_2\text{N}_4$	xx	4.77	3.29	-2.99	-2.68	4.17
	yy	4.77	3.29	-2.99	-2.68	4.17
	zz	0.39	0.83	-0.74	-0.28	1.67
$\text{ZrSi}_2\text{N}_4$	xx	5.02	3.33	-3.16	-2.68	3.96
	yy	5.02	3.33	-3.16	-2.68	3.96
	zz	0.56	0.88	-0.85	-0.30	1.70
$\text{HfSi}_2\text{N}_4$	xx	4.63	3.34	-2.97	-2.69	3.61
	yy	4.63	3.34	-2.97	-2.68	3.61
	zz	0.60	0.89	-0.91	-0.28	1.68

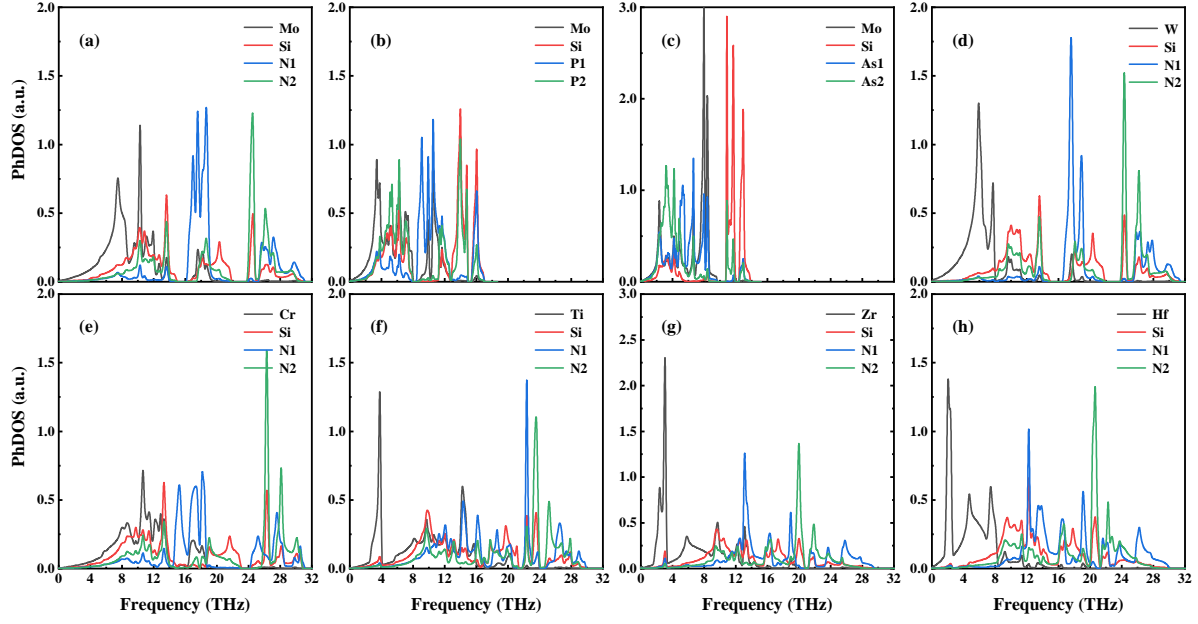


Figure S2. Phonon density of states of  $\text{MSi}_2\text{Z}_4$ : (a)  $\text{MoSi}_2\text{N}_4$ , (b)  $\text{MoSi}_2\text{P}_4$ , (c)  $\text{MoSi}_2\text{As}_4$ , (d)  $\text{WSi}_2\text{N}_4$ , (e)  $\text{CrSi}_2\text{N}_4$ , (f)  $\text{TiSi}_2\text{N}_4$ , (g)  $\text{ZrSi}_2\text{N}_4$  and (h)  $\text{HfSi}_2\text{N}_4$ .

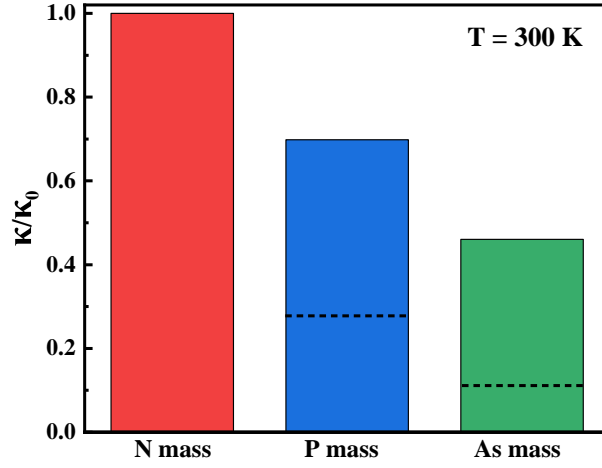


Figure S3. The mass effect of Z atom on the thermal conductivity of  $\text{MoSi}_2\text{Z}_4$  by only changing the mass of N atom to P or As atom in  $\text{MoSi}_2\text{N}_4$ .  $\kappa_0$  and  $\kappa$  are the thermal conductivity of intrinsic and mass substituted  $\text{MoSi}_2\text{N}_4$ , respectively. Dash lines in blue (green) stripe represents the ratio between intrinsic  $\kappa$  of  $\text{MoSi}_2\text{P}_4$  ( $\text{MoSi}_2\text{As}_4$ ) and  $\kappa$  of  $\text{MoSi}_2\text{N}_4$ .

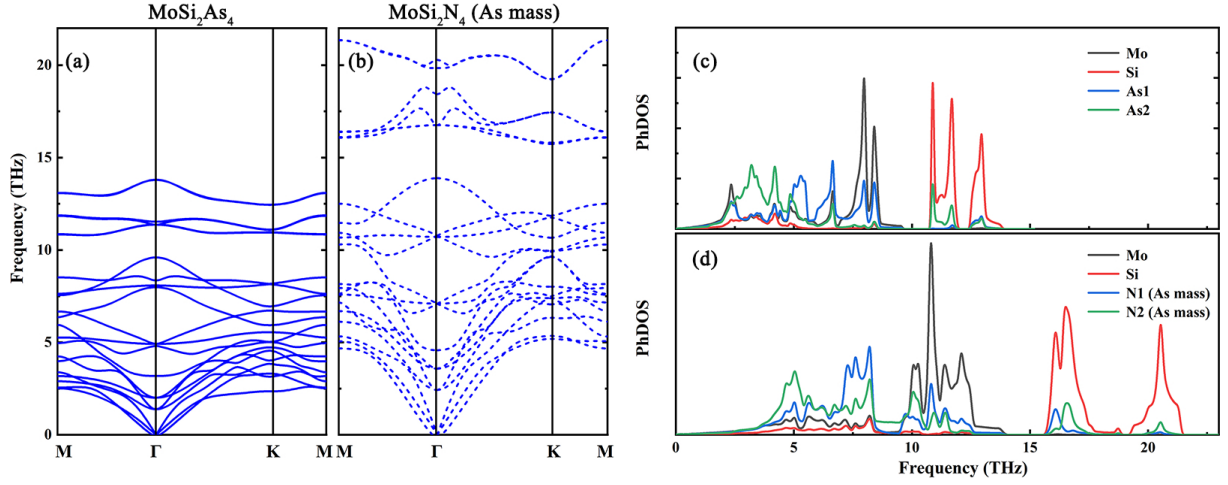


Figure S4. The effect of bond strength induced by Z atom on the phonon dispersion and phonon density of states of MoSi<sub>2</sub>Z<sub>4</sub>. For ensuring mass-independent, the mass of N atom is set as the mass of As atom. (a) and (b) are the phonon dispersion spectrum of MoSi<sub>2</sub>As<sub>4</sub> and MoSi<sub>2</sub>N<sub>4</sub> with As mass, (c) and (d) are the corresponding phonon density of states.

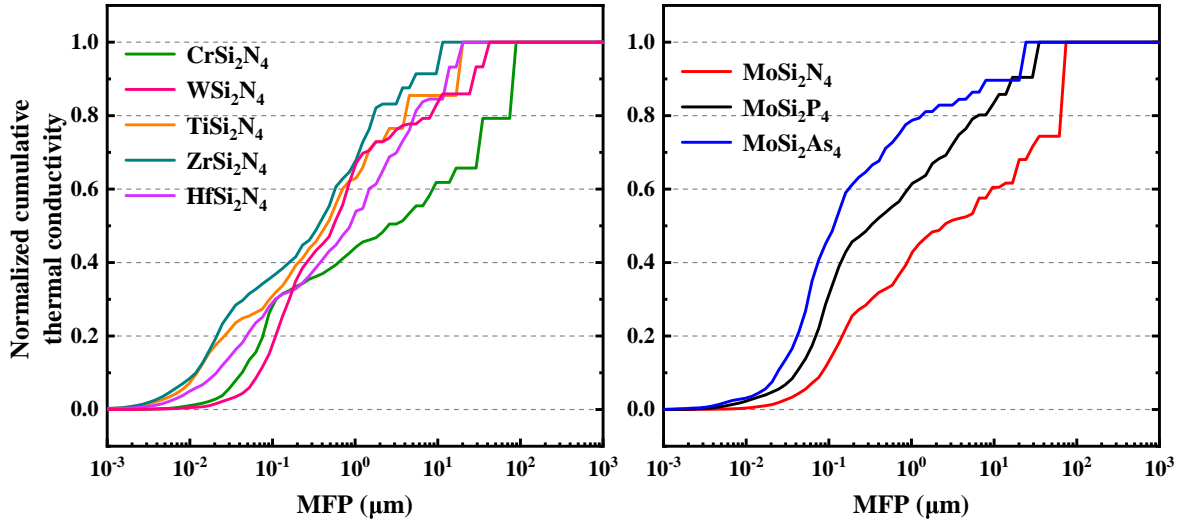


Figure S5. The normalized cumulative thermal conductivity as the function of mean free path (MFP) of CrSi<sub>2</sub>N<sub>4</sub>, WSi<sub>2</sub>N<sub>4</sub>, TiSi<sub>2</sub>N<sub>4</sub>, ZrSi<sub>2</sub>N<sub>4</sub>, HfSi<sub>2</sub>N<sub>4</sub>, MoSi<sub>2</sub>N<sub>4</sub>, MoSi<sub>2</sub>P<sub>4</sub> and MoSi<sub>2</sub>As<sub>4</sub>.

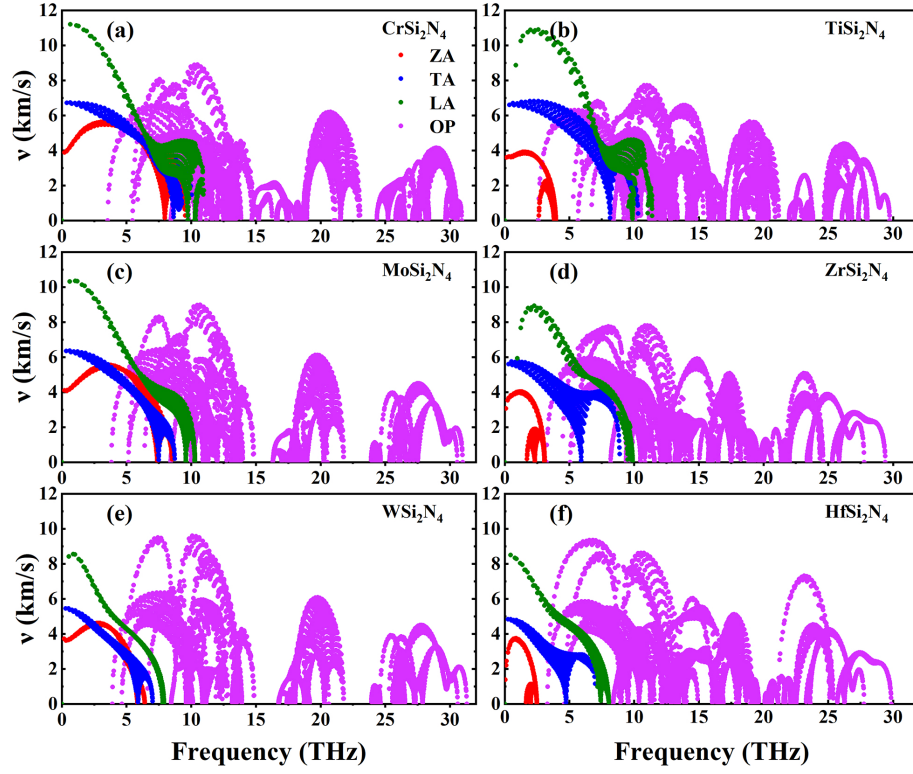


Figure S6. Phonon group velocity of (a)  $\text{CrSi}_2\text{N}_4$ , (b)  $\text{TiSi}_2\text{N}_4$ , (c)  $\text{MoSi}_2\text{N}_4$ , (d)  $\text{ZrSi}_2\text{N}_4$ , (e)  $\text{WSi}_2\text{N}_4$  and (f)  $\text{HfSi}_2\text{N}_4$ .

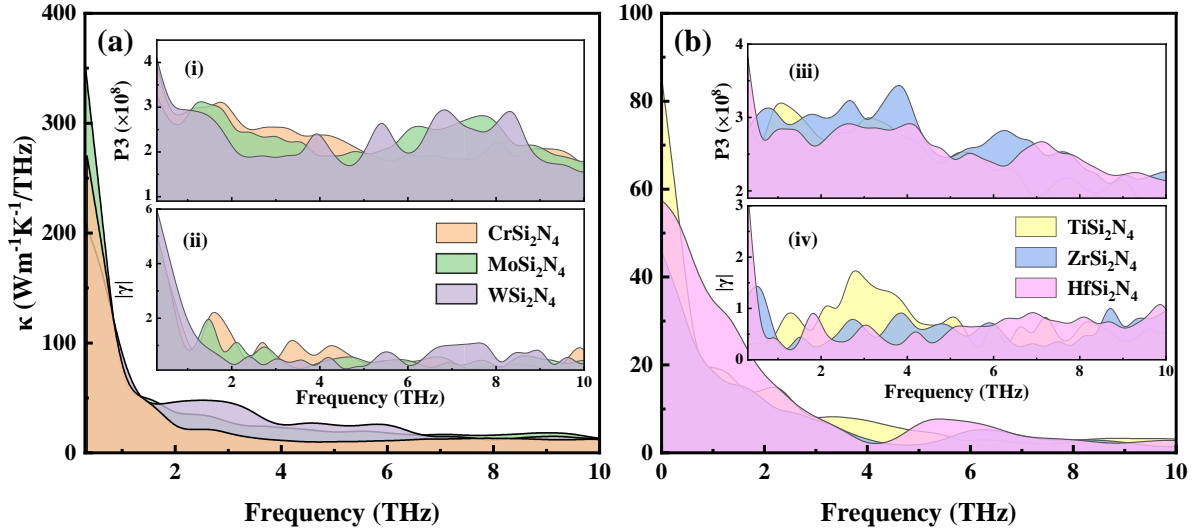


Figure S7. Room-temperature  $\kappa$  as the function of frequency: (a) Group-VIB and (b) Group-IVB  $\text{MSi}_2\text{N}_4$ , the inserted of (i) and (iii) are phase space (P3), (ii) and (iv) are absolute Grüneisen parameter ( $|\gamma|$ ).

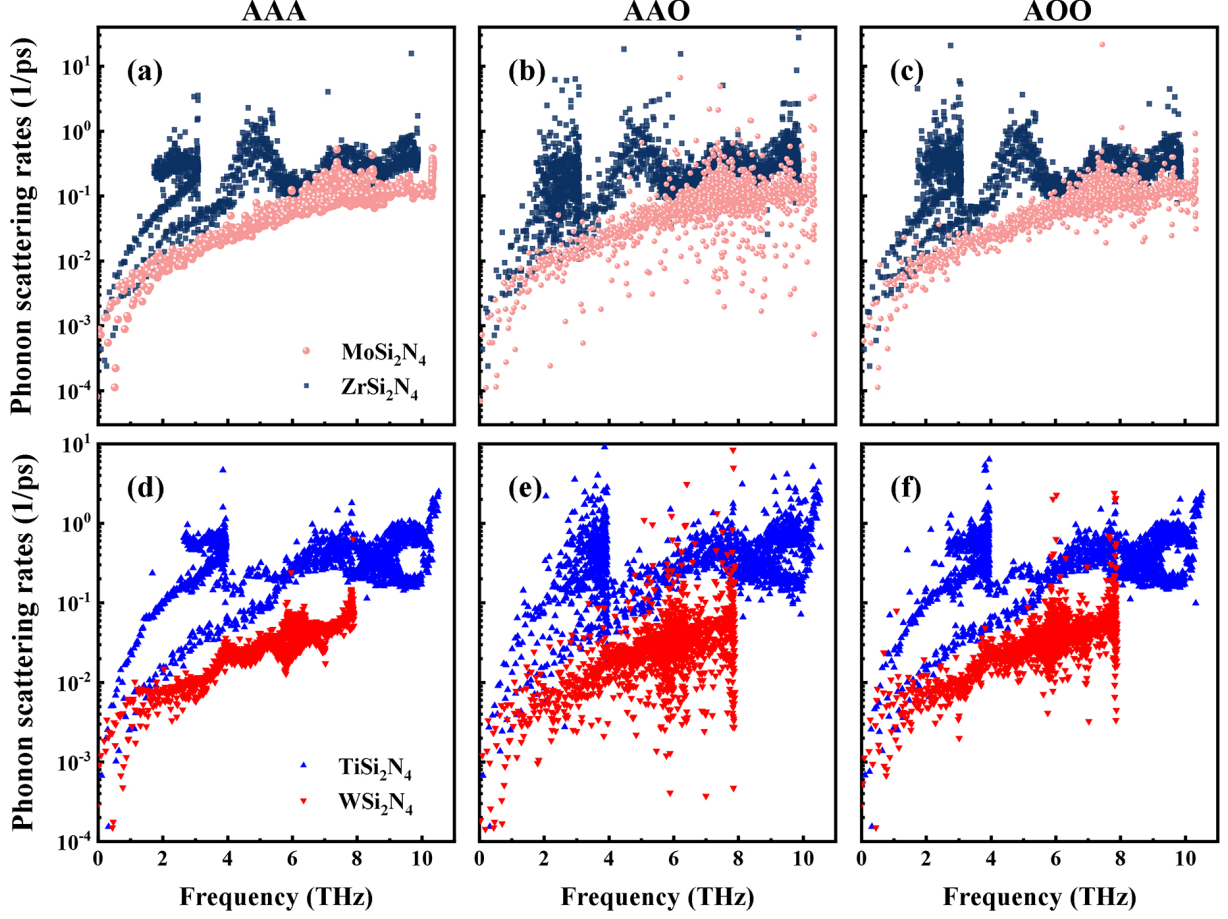


Figure S8. The comparison of phonon scattering rates for particular interacting channels (AAA, AAO and AOO) between (a)–(c) MoSi<sub>2</sub>N<sub>4</sub> and ZrSi<sub>2</sub>N<sub>4</sub>, and between (d)–(f) TiSi<sub>2</sub>N<sub>4</sub> and WSi<sub>2</sub>N<sub>4</sub>.

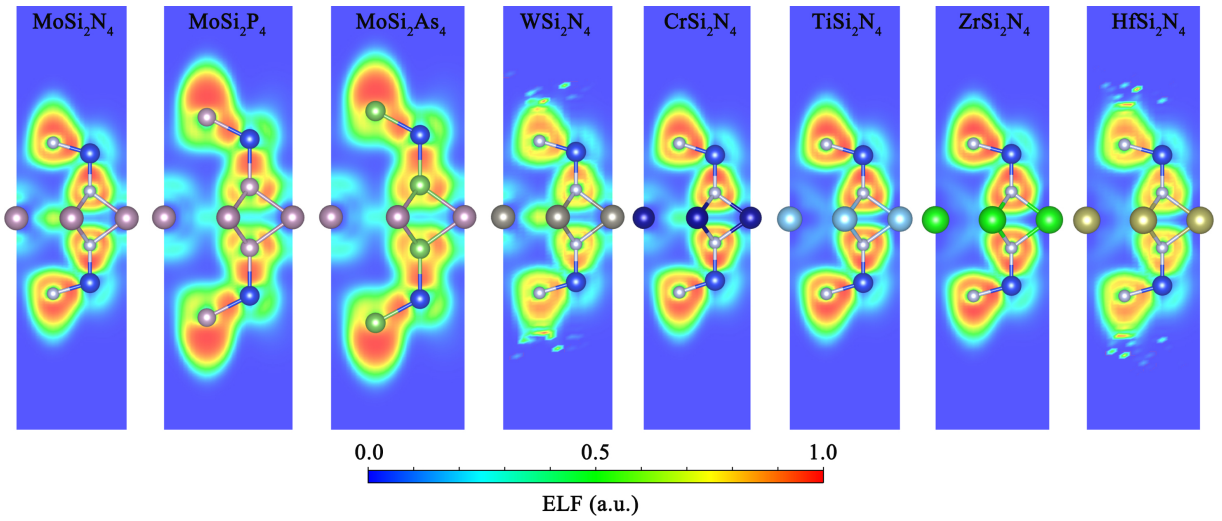


Figure S9. Electron localization function (ELF) distribution of MSi<sub>2</sub>Z<sub>4</sub> in the (110) plane.

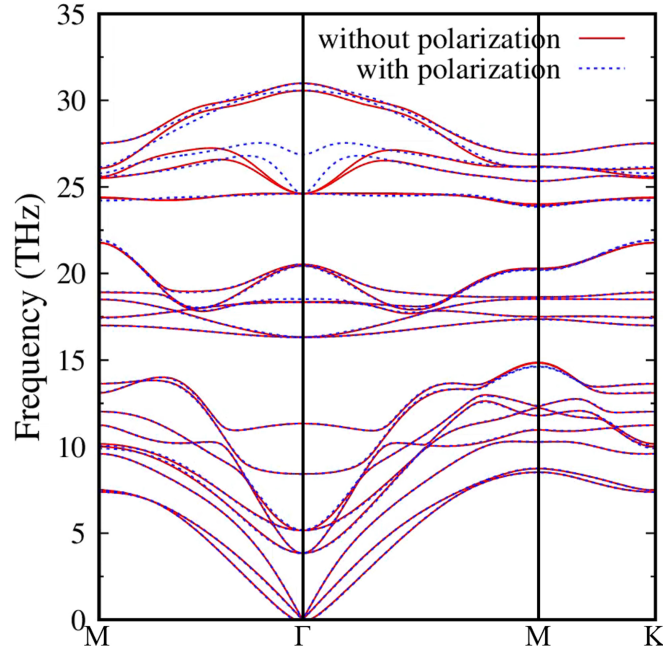


Figure S10. Phonon dispersion spectrum of  $\text{MoSi}_2\text{N}_4$  with (blue dotted line) or without (red solid line) polarization effect.

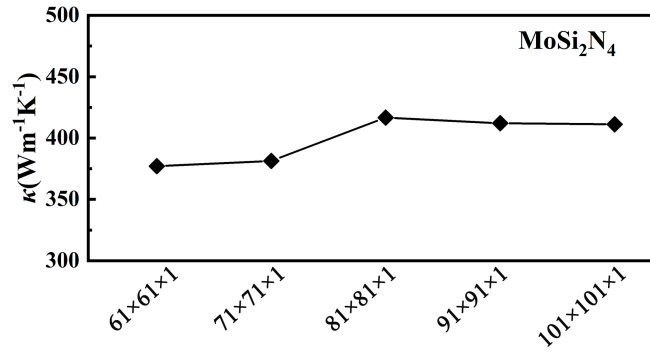


Figure S11. Lattice thermal conductivity ( $\kappa$ ) of  $\text{MoSi}_2\text{N}_4$  as function of grid density from  $61 \times 61 \times 1$  to  $101 \times 101 \times 1$